Title
Rapid and Efficient Arsenic Removal by Iron Electrocoagulation Enabled with in Situ Generation of Hydrogen Peroxide.

Journal
Environmental science & technology, 54(10)

ISSN
0013-936X

Authors
Bandaru, Siva RS
van Genuchten, Case M
Kumar, Arkadeep
et al.

Publication Date
2020-05-01

DOI
10.1021/acs.est.0c00012

Peer reviewed

Manuscript accepted on April 20, 2020 for publication in Environmental Science and Technology.
DOI: 10.1021/acs.est.0c00012

Rapid and efficient arsenic removal by iron electrocoagulation enabled with in-situ generation of hydrogen peroxide

Siva RS Bandaru[†], Case M. van Genuchten[‡], Arkadeep Kumar[§], Sara Glade[†], Dana Hernandez[†], Mohit Nahata[†], Ashok Gadgil [†, §, *]

† Department of Civil and Environmental Engineering, University of California, Berkeley, California 94720-1710, United States

‡ Geologic Survey of Denmark and Greenland, 1350 Copenhagen K, Denmark

§ Energy Technologies Area, Lawrence Berkeley National Laboratory, Berkeley, California 94720, United States

Manuscript accepted on April 20, 2020 for publication in Environmental Science and Technology.
DOI: 10.1021/acs.est.0c00012

Corresponding Author*

E-mail: ajgadgil@lbl.gov; Phone number: (510) 486-4651; Fax: (510) 486-5454

Abstract

Millions of people are exposed to toxic levels of dissolved arsenic in groundwater used for drinking. Iron electrocoagulation (FeEC) has been demonstrated as an effective technology to remove arsenic at an affordable price. However, FeEC requires long operating times (~hours) to remove dissolved arsenic due to inherent kinetics limitations. Air cathode Assisted Iron Electrocoagulation ("ACAIE") overcomes this limitation by cathodically generating H_2O_2 in-situ. In ACAIE operation, rapid oxidation of Fe(II) and complete oxidation and removal of As(III) are achieved. We compare FeEC and ACAIE for removing As(III) from an initial concentration of 1464 µg/L, aiming for a final concentration of less than 4 µg/L. We demonstrate that at short electrolysis times (0.5 minutes), i.e. high charge dosage rates (1200 C/L/min), ACAIE consistently outperformed FeEC in bringing arsenic levels to less than WHO-MCL of 10 µg/L. Using XRD and XAS data, we conclusively show that poor arsenic removal in FeEC arises from incomplete As(III) oxidation, ineffective Fe(II) oxidation and the

Manuscript accepted on April 20, 2020 for publication in Environmental Science and Technology.
DOI: 10.1021/acs.est.0c00012

formation of Fe(II-III) (hydr)oxides at short electrolysis times (<20 minutes). Finally, we report successful ACAIE performance (retention time 19 seconds) in removing dissolved arsenic from contaminated groundwater in rural California.

Manuscript accepted on April 20, 2020 for publication in Environmental Science and Technology.
DOI: 10.1021/acs.est.0c00012

Introduction

Toxic levels of arsenic in groundwater used for drinking is a major public health concern for nearly 200 million people around the world.[1, 2] Chronic exposure to arsenic causes various types of internal cancers, cardiovascular diseases and gangrenes, and low I.Q in children.[3-5] Resource poor communities are adversely impacted by arsenic poisoning due to the lack of affordable and robust solutions.[6-8] Recently, iron electrocoagulation (FeEC) has been demonstrated as an effective, affordable, and robust method to remove arsenic from groundwater both in the laboratory and in extended field trials.[9-11]

In FeEC, a low-voltage direct current applied across low-carbon steel plates immersed into an electrolyte promotes oxidation of Fe(0) to Fe(II) on the Fe anode and reduction of $H_2O/H_{2(g)}$ on the Fe cathode.[12] In-situ generated Fe(II) undergoes further oxidation by dissolved O_2 (DO) in the bulk solution to form insoluble Fe(III) (oxyhydr)oxides.[12] In addition, reactive intermediates (i.e. $^{*}OH$, $^{*}O_2^{-}$, Fe(IV)) generated during oxidation of Fe(II) by O_2 oxidize As(III) to As(V), which is more easily adsorbed than As(III).[13-17] Recent studies report that the charge dosage (CD, C/L), charge dosage rate (CDR, C/L/min) and O_2 recharge rate affect arsenic removal in FeEC for a given electrolyte composition.[18] At a constant CD (C/L), efficient arsenic removal occurs at low CDR because the Fe(II) generation rate becomes lower than the rate of atmospheric O_2 influx into the solution.[18] This allows complete

Manuscript accepted on April 20, 2020 for publication in Environmental Science and Technology.
DOI: 10.1021/acs.est.0c00012

oxidation of dissolved Fe(II) to Fe(III) (oxyhydr)oxides and subsequent removal of arsenic. At higher CDR, imbalance between the rates of Fe(II) generation and O_2 dissolution can result in incomplete oxidation of Fe(II) and formation of the Fe(II-III) (hydr)oxide, green rust, which can be less effective at removing arsenic than Fe(III) precipitates.[19-21] While operating FeEC at low CDR avoids the formation of undesirable green rust in most solutions, low CDR also requires long treatment times (~hours), unattractive for real world applications.

Recently, air diffusion cathodes (herein called “air cathodes”) have been shown to generate H_2O_2 by cathodic reduction of O_2 diffused from air.[22-24] An air cathode comprises a porous carbon cloth with a hydrophobic gas diffusion layer on the air-facing side and a catalyst layer facing the electrolyte. Air cathodes have been shown to produce H_2O_2 at nearly 100% Faradaic efficiency over a wide range of current densities and charge dosage rates.[25, 26] Therefore, replacing the Fe cathode in FeEC, which typically generates $H_{2(g)}$, with an air cathode (technique herein referred to as Air Cathode Assisted Iron Electrocoagulation, or “ACAIE”) results in cathodic H_2O_2 formation. In-situ generated H_2O_2 oxidizes Fe(II) at nearly 4 orders of magnitude faster than O_2 and also produces higher stoichiometric yields of selective reactive intermediates (Fe(IV)) compared to O_2, which enhances the kinetics of As(III) oxidation and removal by orders of magnitude.[13, 27, 28] Processes similar to ACAIE have been reported in the

Manuscript accepted on April 20, 2020 for publication in Environmental Science and Technology.
DOI: 10.1021/acs.est.0c00012

literature under different terms (e.g., electro-Fenton, peroxi-coagulation, etc.) with applications that addressed mainly the removal of persistent organic contaminants at acidic pH via OH radical formation. Only a few studies have examined arsenic removal at circum-neutral pH using ACAIE, but these studies investigated only low CDR operating conditions (2.8 C/L/min) with electrolysis duration of 60 mins, which is prohibitively long for real world applications.[29, 30] These studies also did not examine the structure and arsenic uptake mode of the solids formed in ACAIE, which are expected to be significantly different than those from standard FeEC systems, owing to different pathways and kinetics of their formation. Knowledge of the structure and arsenic bonding mode of the solids formed by ACAIE over a wide range of CDR is essential to predict the arsenic sorption reactivity and colloidal stability of the Fe(III) precipitates and leaching of sorbed arsenic, since the mobilization of arsenic from solids depends on its sorption mode.[19, 31, 32]

In this work, we investigated As(III) removal using FeEC and ACAIE systems over a wide range of operating CDR (1.5 C/L/min to 1200 C/L/min), corresponding to a electrolysis times from 0.5 to 400 minutes and current densities from 0.8 to 156 mA/cm^2. These operating parameters are relevant to decentralized (community scale) and centralized (municipal utility scale) drinking water treatment plants and span the range of parameters used in other industries

Manuscript accepted on April 20, 2020 for publication in Environmental Science and Technology.
DOI: 10.1021/acs.est.0c00012

(inorganic and organic wastewater treatment).[10, 30] We characterized the reaction products in both systems by X-ray diffraction (XRD) and synchrotron-based Fe and As K-edge X-ray absorption spectroscopy (XAS). With these macroscopic and molecular-scale data, we show that ACAIE substantially and consistently outperforms FeEC in removing high concentrations of As(III) to below 4 µg/L as the electrolysis time decreases from hours to minutes (i.e. as CDR increases from 1.5 to >1000 C/L/min). Finally, we demonstrate the performance of a flow-through ACAIE reactor operated at high CDR in a field test using arsenic-contaminated groundwater in a rural community in California. Our results suggest that ACAIE systems can be an attractive alternative to conventional arsenic removal strategies for communities that require rapid flow-through treatment of large volumes of arsenic-contaminated water.

2 Materials and methods

2.1 Laboratory scale electrochemical experiments

2.1.1 FeEC reactor

FeEC experiments were conducted in 0.5 L glass beakers with two parallel low-carbon steel plates (1006-1026 steel grade, McMaster-CARR) separated by a non-conducting spacer (acrylic rectangular sheet: 14 cm × 2.5 cm × 2.5 cm) immersed in the electrolyte. The total submerged surface area of the steel plates in the FeEC experiments was 46 cm^2 (7 cm X 6.5 cm). These plates were cleaned

Manuscript accepted on April 20, 2020 for publication in Environmental Science and Technology.
DOI: 10.1021/acs.est.0c00012

with sandpaper until the surfaces were shiny and then rinsed with deionized water before the experiments.

2.1.2 ACAIE reactor

Laboratory scale ACAIE experiments were performed in a custom-built rectangular batch reactor open to the atmosphere and fitted with a carbon-based air cathode (submerged surface area of 64 cm^2) on one side of the reactor. The air cathodes were fabricated according to Barazesh et al. (2015), with further descriptions in the supporting information (SI).[26] A rectangular steel plate (submerged surface area of 45 cm^2, 1006-1026 steel grade, McMaster-CARR) served as the anode and was placed parallel to the air cathode. A non-conducting spacer (acrylic rectangular sheet: 14 cm × 2.5 cm × 1.3 cm) maintained an inter-electrode distance of 2.5 cm for all ACAIE experiments except for those at CDR of 1200 C/L/min, which were performed at an electrode spacing of 0.7 cm. Images of the 0.5 L ACAIE experimental setup are shown in Figure S1. The same air cathode was used for a single set of charge dosage rate experiments (5 total experiments at CDR of 1.5, 6, 60, 100 and 600 C/L/min). A new air cathode was used to repeat these experiments once and another new air cathode was used to repeat the same experiments a third time. No significant difference in the H_2O_2 Faradaic efficiency of the air cathodes was observed at the beginning and end of each set of replicate experiments (Figure S10A, S10B, S10C).

Manuscript accepted on April 20, 2020 for publication in Environmental Science and Technology.
DOI: 10.1021/acs.est.0c00012

2.1.3 Electrolysis

An external DC power supply operated in galvanostatic mode delivered specified currents to each system. The total charge dosage was 600 C/L (3.1 mM Fe by Faraday's law) unless otherwise specified, which was selected based on the operating parameters of an existing FeEC plant treating arsenic-contaminated groundwater in West Bengal, India.[10, 11] To examine the impact of a wide range of operating conditions on arsenic removal, we varied the electrolysis time from 1 to 400 minutes, which corresponds to CDRs of 600 to 1.5 C/L/min. The volume factor in C/L/min is the actual electrolyte volume being treated. Herein, electrolyte volume and reactor volume are used interchangeably. Additional experiments at an electrolysis time of 0.5 minutes (CDR of 1200 C/L/min) were performed only in the ACAIE system to understand the effect of reduced electrode spacing on arsenic removal and energy consumption.

2.1.4 Electrolyte and measurement protocols

Batches of freshly prepared synthetic Bangladesh groundwater (SBGW, composition listed in Table S1) were used as the electrolyte in all laboratory experiments, unless otherwise noted.[14, 33, 34] SBGW was prepared with reagent grade chemicals and is described further in the SI. The initial pH of each experiment was adjusted to 7.0 by bubbling $CO_{2(g)}$ or by adding small volumes of 1.1 M HCl or 1 M NaOH. The electrolyte was stirred (~550 rpm) with a magnetic stir plate during

Manuscript accepted on April 20, 2020 for publication in Environmental Science and Technology.
DOI: 10.1021/acs.est.0c00012

electrolysis. At the end of electrolysis, unfiltered and filtered (0.45 μm Nylon filter) samples were collected to measure total and dissolved concentrations of constituents. Herein, the constituents measured in the filtrate are referred to as “dissolved concentrations”. The initial and final pH, DO and conductivity were measured using an Orion Star™ A329 meter. Dissolved arsenic and iron concentrations were measured by ICP-MS (Agilent 7700) and the concentrations of total Fe, P, Ca, Mg and Si in the initial electrolytes were measured by ICP-OES (PerkinElmer 5300 DV). New air cathodes were characterized for H_2O_2 generation before use in ACAIE experiments (see SI for experimental details). All laboratory experiments were performed in triplicates at room temperature; error bars represent the standard deviation of the measurements.

2.2 Field scale ACAIE experiments

Field experiments were performed with local arsenic-contaminated groundwater at a farm in rural community in California using a custom flow-through ACAIE reactor with high surface area (FigureS2). The primary goal of this field trial was to test the effectiveness of ACAIE at intermediate scales in some worst-case scenario conditions (i.e. short retention times) and it was not our goal to test this prototype over extended periods. In this ACAIE system, an air cathode and low-carbon steel anode (1006-1026 steel grade, McMaster-CARR), each with a submerged surface area of 400 cm^2,

Manuscript accepted on April 20, 2020 for publication in Environmental Science and Technology.
DOI: 10.1021/acs.est.0c00012

were positioned at an inter-electrode spacing of 1 cm. A stainless-steel mesh (316 stainless steel wire cloth, 20 x 20 mesh size, 0.07 cm opening size, wire diameter 0.06 cm) was used on the air-facing side of the air cathode to act as a current collector and provide mechanical support. Additional mechanical support to the air cathode and stainless-steel mesh assembly was provided by a 1.3 cm thick acrylic sheet with holes to access air, as shown in Figure S2A. This system was operated at a flow rate of 1.3 L/min and with a hydraulic retention time of 19 seconds. The actual electrolyte volume or reactor volume of this reactor was 0.4 L. The CD and CDR employed in the field were 233 C/L and 750 C/L/min. Samples for total and dissolved concentrations were collected every five minutes at the outlet. The experiment was stopped after treating 100 L of arsenic-contaminated groundwater (250 equivalent reactor volumes). At the end of electrolysis, commercial grade alum (5 mg/L as Al) was added as a coagulant to the 100 L of treated water and allowed to flocculate for another 20 minutes. After flocculation, samples for measurement of dissolved arsenic were collected by filtering an aliquot of treated water through a 0.45 µm filter.

2.3 X-ray diffraction

Experiments for XRD characterization were conducted using the FeEC and ACAIE experimental setups described in sections 2.1.1 and 2.1.2, but a simple electrolyte (5 mM NaCl, 5 mM $NaHCO_3$, pH 7) was

Manuscript accepted on April 20, 2020 for publication in Environmental Science and Technology.
DOI: 10.1021/acs.est.0c00012

used instead of SBGW. We used the simple electrolyte, which was free of surface-poisoning oxyanions, to ensure that the solids formed were crystalline enough for adequate characterization by XRD. For this analysis, we focused primarily on distinguishing between pure Fe(III) precipitates and mixed-valent Fe(II-III) (hydr)oxides. Fe precipitates for XRD measurements were collected on a 0.1 μm filter using a vacuum pump. Fe(II-III) (hydr)oxide samples were collected under nitrogen atmosphere and a small amount (~1mL) of glycerol was added to the filtered solids to prevent Fe(II) oxidation by exposure to air.[35] Diffractograms were collected from 5˚ to 95˚ 2θ with a Bruker AXS D8 Discover GADDS X-ray diffractometer, using Co K-α radiation. To facilitate comparison among samples with different crystallinity, we report the diffractograms normalized by the highest intensity peak.

2.4 X-ray absorption spectroscopy

Fe and As K-edge X-ray absorption spectra were collected at beam line 4-1 of the Stanford Synchrotron Radiation Lightsource (SSRL, Menlo Park, USA). Fe K-edge spectra were recorded at room temperature in transmission mode out to *k* of 13 $Å^{-1}$ using ion chambers to measure I_0 and I_t. As K-edge spectra were recorded at liquid nitrogen temperatures (≈80 °K) in fluorescence mode out to *k* of 13.5 or 14 $Å^{-1}$ using a Lytle detector. Individual spectra were aligned, averaged, and background-subtracted using SixPack software[36] following standard methods described previously.[37] The EXAFS spectra

Manuscript accepted on April 20, 2020 for publication in Environmental Science and Technology.
DOI: 10.1021/acs.est.0c00012

were extracted using k^3-weighting and the As K-edge EXAFS spectra were Fourier-transformed over the k-range 4 to 13 $Å^{-1}$ using a Kaiser-Bessel window with dk of 3 $Å^{-1}$. Additional details regarding the sample preparation and data collection procedures are given in the SI.

2.4.1 As K-edge XANES analysis

The percentages of As(III) and As(V) in each sample were quantified by linear combination fits (LCFs) of the As K-edge XANES spectra using the SixPack software.[36] To minimize systematic errors due to the selection of particular reference compounds, we preformed three sets of LCFs for each sample using three sets of As(III) and As(V) adsorption reference spectra: As(III) and As(V) adsorbed to 2-line ferrihydrite, magnetite and green rust. The details of the synthesis and data collection of these reference spectra are described elsewhere.[19, 38] The XANES LCFs were performed over the range of 11860 to 11880 eV, with negative percentages disallowed. Individual LCFs were not constrained to sum the percentages of fit-derived As(III) and As(V) to 100. We report the As(III) and As(V) percentages in the samples as the average and standard deviation of the three sets of LCFs.

2.4.2 As K-edge EXAFS shell-by-shell fits

Theoretical curve fits of the As K-edge EXAFS spectra of select samples and adsorption references were carried out in $R+\Delta R$-space (Å) using the SixPack software,[36] which is built on algorithms derived from the IFEFFIT library.[39] The presence of multiple arsenic oxidation states

Manuscript accepted on April 20, 2020 for publication in Environmental Science and Technology.
DOI: 10.1021/acs.est.0c00012

bound to the solids can lead to the co-existence of several distinct coordination complexes and multiple scattering paths, each with different fitting parameters.[40] Therefore, to simplify our analysis, we only performed shell-by-shell fits on samples determined by XANES analysis to contain a single oxidation state (i.e. >90% As(III) or As(V)). Phase and amplitude functions (As-O, As-O-O, As-Fe) were calculated with FEFF6[41] using the crystal structure of scorodite.[42] We geometrically constrained the As-O-O multiple-scattering path in the fits to the first-shell As-O path and set its degeneracy to 12 for samples containing As(V) and 6 for samples containing As(III). Further details of the shell-by-shell fitting approach are given in the SI.

3 Results

3.1 Behavior of bulk solution parameters in FeEC and ACAIE systems

3.1.1 Arsenic removal

Manuscript accepted on April 20, 2020 for publication in Environmental Science and Technology.
DOI: 10.1021/acs.est.0c00012

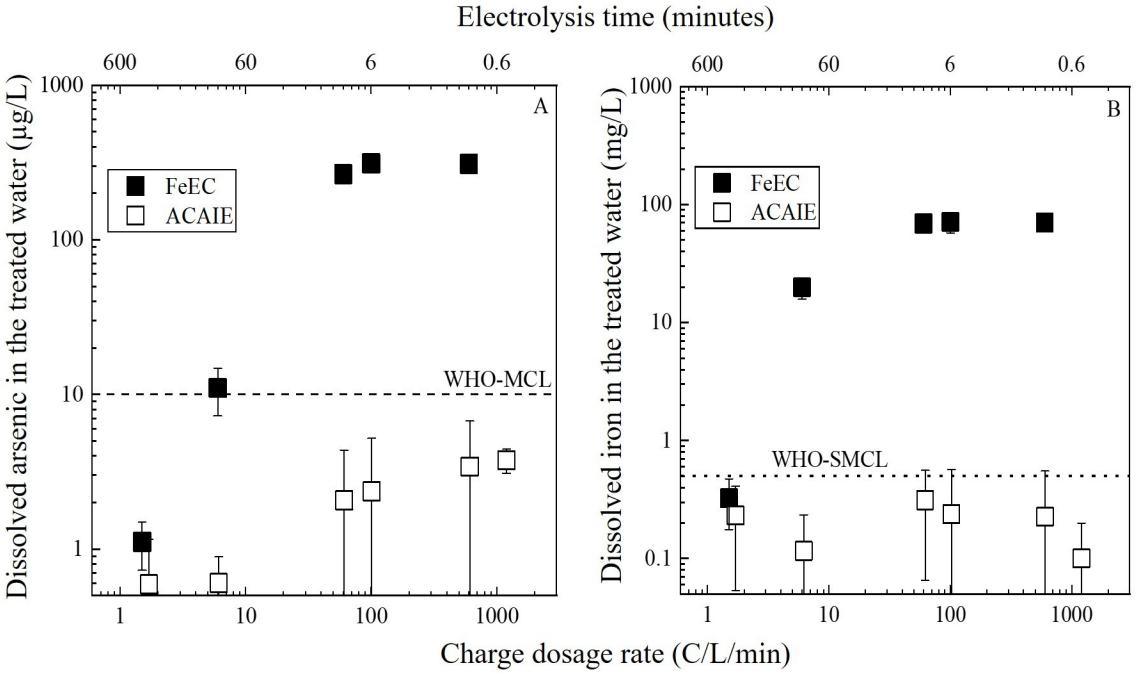

Figure 1: Dissolved arsenic (A) and iron (B) remaining in the filtered solution after electrolysis as a function of CDR in the FeEC (black squares) and ACAIE (white squares) systems. The corresponding electrolysis times are shown in the secondary X-axis above (note decreasing values from left to right). The total charge dosage in each experiment was 600 C/L. Synthetic Bangladesh groundwater was used as the electrolyte (initial As(III) of 1464 ± 83 µg/L).

Figure 1A shows the effect of CDR on the residual arsenic in solution after treatment in the FeEC and ACAIE systems for a total charge dose of 600 C/L (3.1 mM Fe by Faraday's law). In the FeEC system, the residual arsenic was less than 10 µg/L at the lowest CDR of 1.5 C/L/min, but increased to slightly more than 10 µg/L as the CDR increased to 6 C/L/min. Dissolved arsenic levels after treatment increased substantially when the CDR was increased further, leading to 20 times more aqueous arsenic (>200 µg/L) for all FeEC experiments

Manuscript accepted on April 20, 2020 for publication in Environmental Science and Technology.
DOI: 10.1021/acs.est.0c00012

at CDR >6 C/L/min. Aqueous arsenic in the treated water in the FeEC system was never below 300 µg/L in experiments at the highest CDRs of 100 to 600 C/L/min. In sharp contrast, the residual arsenic levels in the ACAIE experiments depended less on CDR and were below 4 µg/L for all experiments (white squares in Figure 1A). In ACAIE experiments, dissolved arsenic in the treated water increased slightly from 0.6 ± 0.6 µg/L to 3.8 ± 0.7 µg/L across the entire range of CDRs from 1.5 to 1200 C/L/min, which corresponds to electrolysis times ranging from 400 to 0.5 minutes.

Figure 1B shows the influence of CDR on the dissolved iron concentration immediately after electrolysis in the FeEC and ACAIE systems. For FeEC experiments, the dissolved iron concentration increased from 0.3 mg/L to 20 mg/L with an increase in CDR from 1.5 to 6 C/L/min, but then stabilized at 70 mg/L at CDR ≥ 60 C/L/min. The aqueous iron levels were also significantly lower using an air cathode compared to an Fe cathode. In all ACAIE experiments, regardless of CDR, the dissolved iron remained below the WHO Secondary MCL (WHO-SMCL) of 0.3 mg/L.

3.1.2 pH and DO

The average initial pH in both FeEC and ACAIE experiments was 7.0 ± 0.1. The final pH in FeEC and ACAIE experiments behaved differently with CDR. The final pH in all FeEC experiments was always at least 0.5 log units higher than the initial value and ranged from 7.6

Manuscript accepted on April 20, 2020 for publication in Environmental Science and Technology.
DOI: 10.1021/acs.est.0c00012

to 7.9 (Figure S3A). In ACAIE experiments, the final pH also increased from the initial value, but a more systematic trend with CDR was observed. At the lowest CDR of 1.5 C/L/min, the final pH was 7.8, whereas the final pH was only 7.1 at the highest CDR of 1200 C/L/min, which corresponds to the shortest electrolysis time of 0.5 minutes.

The average initial DO in FeEC and ACAIE experiments was 7.4 ± 1.0 mg/L. The behavior of final DO differed significantly in the FeEC and ACAIE experiments (Figure S3B). In the FeEC system, the DO decreased substantially after treatment. The final DO was 3.5 mg/L when the CDR was 1.5 C/L/min, and it decreased further as CDR increased, leading to a DO of <0.1 mg/L for experiments at CDR ≥ 6 C/L/min. In contrast, the final DO in the ACAIE system was higher than the initial value. The final DO increased from 8.7 to 11.7 mg/L with an increase in CDR from 1.5 to 100 C/L/min, but dropped to 8.8 and 7.9 mg/L at CDR of 600 and 1200 C/L/min.

3.1.3 Color and total iron concentrations of the suspension

After electrolysis, visual inspection the electrolyte in FeEC experiments showed orange precipitates at CDR of 1.5 C/L/min, consistent with Fe(III) (oxyhydr)oxides, and the characteristic green-ish blue color of green rust (GR) for experiments at CDR ≥ 6 C/L/min (Figure S4). Measurements of total iron in suspension indicated the total iron produced was more than 90% of the theoretical value based on Faraday's law at all CDRs except at 1.5 C/L/min, where only 82% of

Manuscript accepted on April 20, 2020 for publication in Environmental Science and Technology.
DOI: 10.1021/acs.est.0c00012

the theoretical iron concentration was observed. In contrast to FeEC experiments, only orange precipitates were observed in the ACAIE system at all CDRs. Furthermore, the total iron measured in the ACAIE experiments was >95% of the theoretical value at all CDRs (Figure S5).

The efficiency of H_2O_2 production by the air cathodes used in the ACAIE experiments (Figure S6) was lowest at the lowest CDR of 1.5 C/L/min (48 ± 9% of the theoretical value), but increased steadily with increasing CDR (>80% of the theoretical H_2O_2 at CDR> 60 C/L/min).

3.2 Structure of iron precipitates formed in FeEC and ACAIE systems

3.2.1 X-ray diffraction

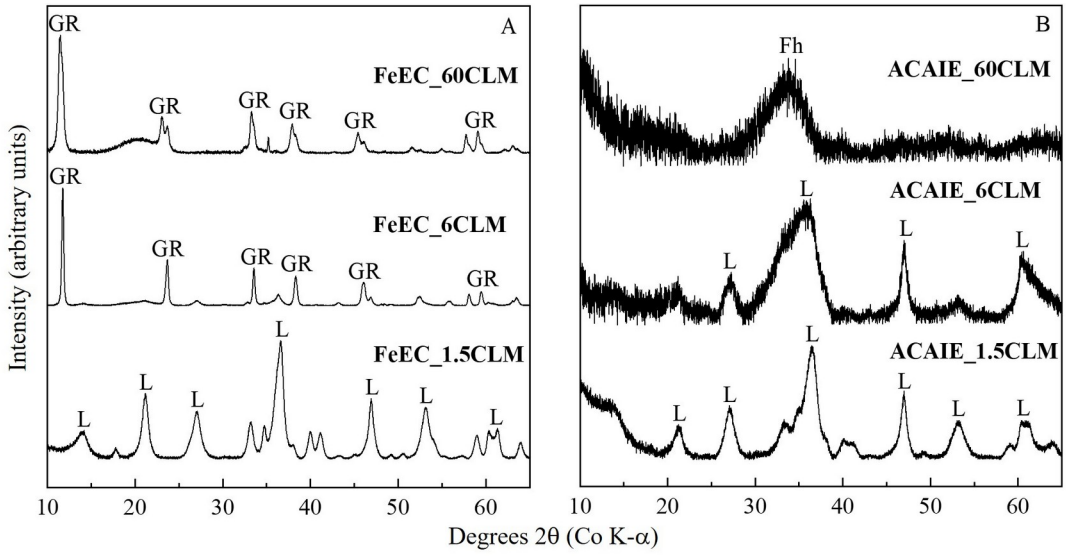

Figure 2: XRD patterns of the Fe precipitates collected after electrolysis in FeEC (A) and ACAIE (B) systems. The electrolyte was 5 mM NaCl + 5 mM $NaHCO_3$ (pH 7). The letters L, Fh and GR indicate the diffraction peaks of lepidocrocite, ferrihydrite and carbonate green rust respectively.[43-46] CLM in the figures represents C/L/min. The broad peak near 21° 2θ in Figure 2A arises from glycerol.

Manuscript accepted on April 20, 2020 for publication in Environmental Science and Technology.
DOI: 10.1021/acs.est.0c00012

The diffractograms of the Fe precipitates in the FeEC and ACAIE systems showed different characteristic Bragg peaks depending on CDR (Figure 2). At low CDR, diffraction peaks from lepidocrocite were observed in the FeEC system, consistent with the orange color of the solids. However, as the CDR increased to 6 and 60 C/L/min, characteristic Bragg peaks of carbonate GR were observed in the solids, with intense reflections near 12° 2θ and 24° 2θ. In addition, the GR formed at 60 C/L/min had broader peaks than the 6 C/L/min sample, consistent with its 10-fold shorter synthesis time. The XRD patterns of the solids formed in the ACAIE experiments showed systematic trends with CDR, but the changes in peak position and intensity were different than those in the FeEC system. At CDR of 1.5 C/L/min, peaks consistent with lepidocrocite were observed, but the peaks were broader than those at the same CDR in the FeEC system. As the CDR increased from 1.5 to 60 C/L/min in the ACAIE system, the diffraction patterns showed a progressive decrease in peaks arising from lepidocrocite to peaks consistent with 2-line ferrihydrite (2LFh). Similar to the FeEC system, the highest CDR in the ACAIE system formed solids with the lowest crystallinity, but no evidence for mixed-valent Fe(II-III) (hydr)oxides were observed.

3.2.2 Fe K-edge XANES and EXAFS

Manuscript accepted on April 20, 2020 for publication in Environmental Science and Technology.
DOI: 10.1021/acs.est.0c00012

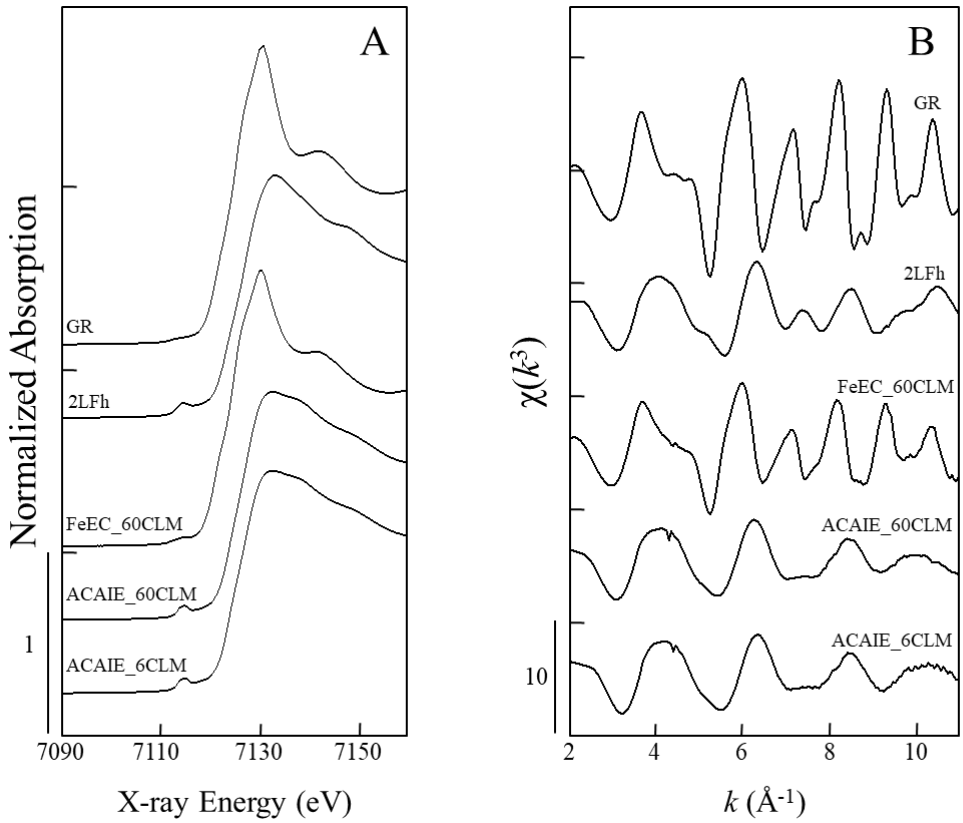

Figure 3: Fe K-edge XANES (A) and EXAFS spectra (B) of the Fe precipitates formed in FeEC and ACAIE systems. Reference spectra for green rust (GR) and 2-line ferrihydrite (2LFh) are also give for comparison. SBGW was used as the electrolyte in these experiments. CLM represents C/L/min.

The Fe K-edge XANES and EXAFS spectra of the Fe precipitates formed in FeEC and ACAIE systems are compared to the spectra of Fe-bearing reference minerals (e.g. GR and 2LFh) in Figure 3. Consistent with the XRD data, the line shape of the XANES spectrum of solids produced at 60 C/L/min in the FeEC system matched the GR reference spectrum (Figure 3A), particularly the sharp absorption peak near 7130 eV. In addition, the EXAFS spectrum of this sample resembled the EXAFS spectrum of GR, including the asymmetric first oscillation from

Manuscript accepted on April 20, 2020 for publication in Environmental Science and Technology.
DOI: 10.1021/acs.est.0c00012

2.5 to 4.5 $Å^{-1}$. However, the EXAFS oscillations of the FeEC 60 C/L/min sample had lower amplitude and were more broad than the GR reference spectrum, which can be explained by the FeEC sample having lower crystallinity than the reference GR due to its rapid synthesis time and formation in the presence of surface-poisoning ions.

In contrast to the FeEC system, the ACAIE samples (6 and 60 C/L/min) yielded solids with XANES spectra that matched closely that of 2LFh. The more intense pre-edge peak and the flattened region near the absorption maximum, which is also found in the spectrum of 2LFh, indicate the predominance of Fe(III) in the ACAIE samples, consistent with the XRD patterns. The EXAFS spectra of the ACAIE samples also matched that of 2LFh, particularly the symmetric first oscillation and low amplitude peaks at $k > 8$ $Å^{-1}$. However, some subtle differences are apparent between the EXAFS spectra of 2LFh and the ACAIE samples. For example, the small shoulder in the first oscillation near 5.5 $Å^{-1}$ in the 2LFh EXAFS spectrum is reduced in the ACAIE samples and the small peak near 7.5 $Å^{-1}$ is flat in the ACAIE samples. These differences are consistent with a lower degree of edge- and corner-sharing bonding in the ACAIE samples relative to 2LFh.[47]

3.3 As X-edge X-ray absorption spectroscopy

3.3.1 As K-edge XANES spectra

Manuscript accepted on April 20, 2020 for publication in Environmental Science and Technology.
DOI: 10.1021/acs.est.0c00012

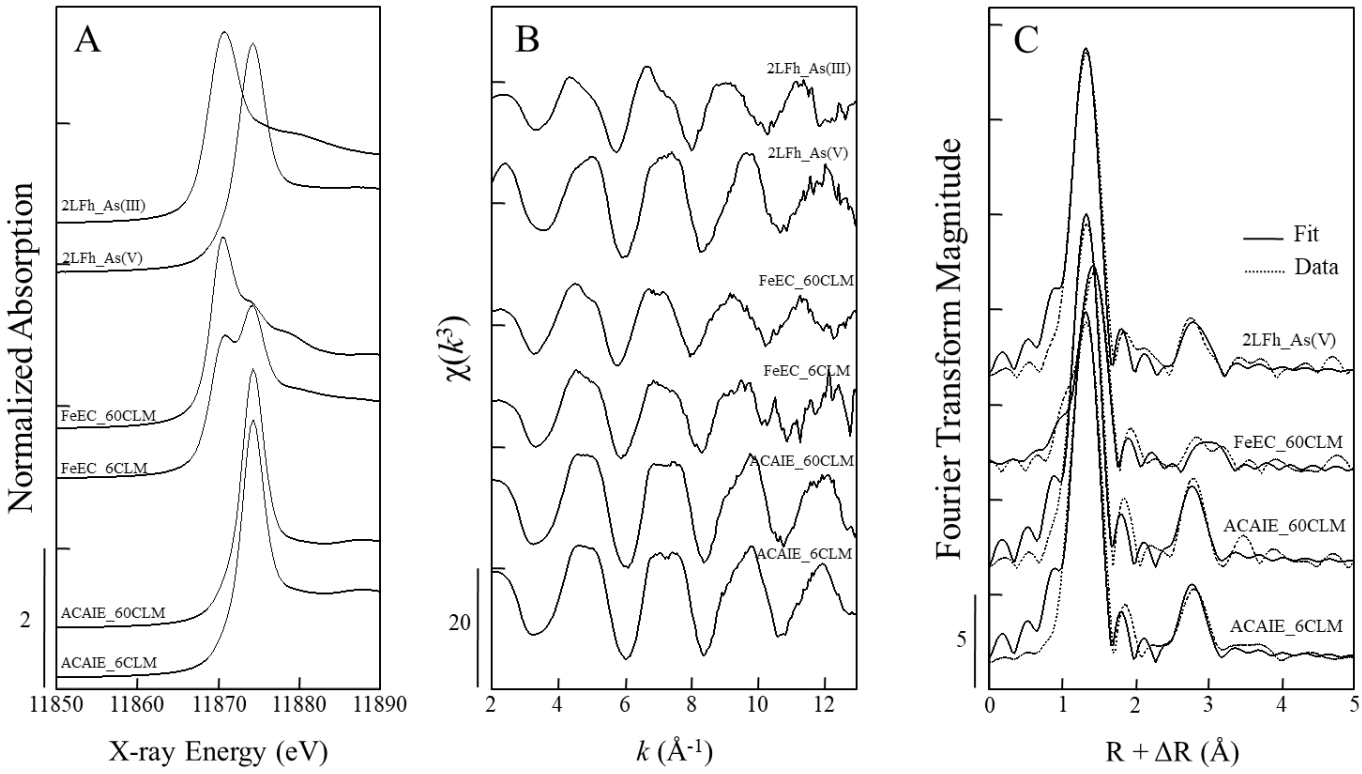

Figure 4: As K-edge XANES (A), EXAFS (B), and corresponding Fourier transforms (C) of FeEC and ACAIE samples. Reference spectra of As(III) and As(V) adsorbed to 2-line ferrihydrite (2LFh_As(III), 2LFh_As(V)) are also given. In C), the shell-by-shell fitting output is given in solid lines and the data is given in dotted lines. SBGW was used as the electrolyte in these experiments. CLM represents C/L/min.

Figure 4A compares the As K-edge XANES spectra of solids formed in the FeEC and ACAIE systems at CDRs of 6 and 60 C/L/min to the reference spectra of As(III) and As(V) adsorbed to 2LFh. In the FeEC system, the XANES spectrum of the solids formed at 6 C/L/min has two distinct peaks with maxima near 11870 eV and 11874 eV, consistent with the absorption maxima for the reference As(III) and As(V) spectra. At increased CDR in the FeEC system, the peak indicative of As(III) increases and is accompanied by a nearly complete decrease in the

Manuscript accepted on April 20, 2020 for publication in Environmental Science and Technology.
DOI: 10.1021/acs.est.0c00012

As(V) peak. The LCFs of these samples (Table S2) confirm that the As(III) percentage increases from 63 ± 2% to 100 ± 2% as the CDR increases from 6 to 60 C/L/min, indicating inefficient As(III) oxidation at high CDR in the FeEC system. By contrast, only peaks for As(V) are apparent in the XANES spectra of samples produced at identical CDRs of 6 and 60 C/L/min in the ACAIE system. The LCFs of the ACAIE samples revealed a negligible percentage of As(III), with only As(V) detected, which indicates highly effective As(III) oxidation using an air cathode, even at high CDR values.

3.3.2 As K-edge EXAFS spectra

Figure 4B displays the As K-edge EXAFS spectra of samples produced at CDR of 6 and 60 C/L/min in the FeEC and ACAIE systems. In the FeEC system, the EXAFS oscillations of the samples resembled the As(III) adsorption reference spectrum, consistent with the XANES LCFs indicating the predominance of sorbed As(III). The first two oscillations from 4 to 8 $Å^{-1}$ in the FeEC samples showed a small, asymmetric shoulder at higher *k*, which is also present in the As(III) adsorption reference. The EXAFS spectra of samples in the ACAIE system are characterized by flatter oscillations from 4 to 8 $Å^{-1}$ than the FeEC samples and the reference spectra. Compared to the reference spectra, the ACAIE samples are a closer match to As(V) adsorbed to 2LFh, which is consistent with the absence of As(III) determined by XANES LCFs.

Manuscript accepted on April 20, 2020 for publication in Environmental Science and Technology.
DOI: 10.1021/acs.est.0c00012

3.3.3 Shell-by-shell fits of the As K-edge EXAFS Spectra

Figure 4C shows the Fourier-transformed As K-edge EXAFS spectra of select FeEC and ACAIE samples and reference spectra with the output of the shell-by-shell fits overlain on the data. The results of the shell-by-shell fits are given in Table S2. For the FeEC sample at CDR of 60 C/L/min, which was determined to be >95% As(III) by XANES LCFs, the first-shell fits were consistent with As(III) based on the fit-derived coordination number (CN_{As-O}) of 3.1 ± 0.4 and interatomic distance (R_{As-O}) of 1.77 ± 0.01 Å.[48] The second shell of this sample was fit with an As-Fe path with CN = 1.3 ± 0.6 and R = 3.41 ± 0.03 Å. This R_{As-Fe} value is identical within fit-derived errors to previous studies assigning this interatomic distance to As(III) bound in a binuclear corner-sharing (^{2}C) geometry to GR particle edges.[40] However, we note that the fit-derived CN_{As-Fe} value of 1.3 ± 0.6 is slightly lower than the theoretical value of 2.0 for the ^{2}C geometry. Attempts to fit the second shell with an As-Fe mononuclear edge-sharing (^{2}E) bond with R_{As-Fe} near 3.0 Å, which has been proposed in previous studies of As(III) bound to Fe precipitates,[48] were unsuccessful, yielding physically meaningless (or negative) values of CN_{As-Fe} and R_{As-Fe}.

Fits of the first and second shells of the solids formed in the ACAIE system at CDR of 6 and 60 C/L/min were similar, indicating a similar arsenic uptake mode regardless of CDR. The first shell As-O parameters returned by the fit were CN_{As-O} of 4.4 ± 0.5 to 4.7 ± 0.5 and

Manuscript accepted on April 20, 2020 for publication in Environmental Science and Technology.
DOI: 10.1021/acs.est.0c00012

498 R_{As-O} of 1.69 ± 0.01 Å, consistent with As(V) in tetrahedral
499 coordination.[49] The second-shell fits in the ACAIE system yielded values
500 of 3.0 ± 0.8 to 3.1 ± 0.8 for CN_{As-Fe} and 3.24 ± 0.02 Å for R_{As-Fe}. These
501 second-shell fitting parameters are similar to those of the reference
502 spectrum of As(V) adsorbed to 2LFh (CN_{As-Fe} =1.9 ± 0.9; R_{As-Fe} = 3.28 ±
503 0.03 Å), but the ACAIE samples have a slightly higher CN. Based on
504 the R_{As-Fe} of 3.24 Å for ACAIE samples, we conclude that As(V) is bound
505 to the ACAIE solids in the ^{2}C geometry.[49] The R_{As-Fe} of the ACAIE
506 samples (3.24 Å) is almost 0.2 Å shorter than the R_{As-Fe} of the FeEC
507 sample at CDR of 60 C/L/min (3.41 Å), which we identified as As(III)
508 bound also in the ^{2}C geometry. This difference in R_{As-Fe} for the same ^{2}C
509 geometry reflects the shorter As-O distance of As(V) (1.69 Å) compared
510 to As(III) (1.77 Å) and the shorter average Fe-O distance (2.0 Å) for
511 Fe(III) precipitates[50] compared to GR (2.1 Å).[51]

512 **3.4 Field performance of a flow through ACAIE in rural**
513 **California**

514 Figure S7 shows the arsenic removal performance of the
515 continuous flow ACAIE system that treated 100 L (250 equivalent
516 reactor volumes, 19 second retention time) of real groundwater
517 followed by coagulation and flocculation. Pre-coagulation filtered
518 samples, collected during electrolysis, had a pale-yellow color
519 indicative of particulate Fe, which suggests arsenic-bearing Fe(III)
520 precipitates of sizes smaller than 0.45 µm passed through the filter.

Manuscript accepted on April 20, 2020 for publication in Environmental Science and Technology.
DOI: 10.1021/acs.est.0c00012

Therefore, we measured dissolved iron concentrations above 0.3 mg/L (WHO-SMCL) during electrolysis. Dissolved iron reached below 0.3 mg/L after coagulation and flocculation with alum (5 mg/L as Al). Dissolved arsenic concentrations decreased dramatically from an initial value of 118 µg/L to less than 30 µg/L in the first five minutes and then remained below 20 µg/L, when collected during electrolysis. After flocculation, dissolved arsenic decreased to below 0.5 µg/L.

4 Discussions

4.1 Impact of CDR on the structure of Fe precipitates in the FeEC and ACAIE systems

In FeEC, complete oxidation of Fe(II) to Fe(III) is achieved when the rate of Fe(II) generation is less than rate of atmospheric O_2 dissolution; this typically occurs at low CDR. At a low CDR of 1.5 C/L/min, completely oxidized Fe(III) precipitates formed in FeEC, which is consistent with the final DO near 3.5 mg/L (Figure S3B). At increased CDR, measurements of the final DO below 0.1 mg/L indicate that the rate of Fe(II) generation exceeded the rate of O_2 dissolution. This rapid introduction of Fe(II) and consumption of DO at CDR ≥6 C/L/min resulted in incomplete Fe(II) oxidation and the formation of GR. This conclusion is supported by the XRD and Fe K-edge XAS data as well as the characteristic color of solids.

In contrast to the FeEC system, complete oxidation of Fe(II) to Fe(III) during ACAIE treatment occurred due to the nearly equimolar

Manuscript accepted on April 20, 2020 for publication in Environmental Science and Technology.
DOI: 10.1021/acs.est.0c00012

generation of H_2O_2 by the cathode, especially at high CDR (80-85% efficiency, Figure S6).[26] In addition, the H_2O_2 Faradaic efficiency remained nearly constant (~85 %) even when the CDR increased an order of magnitude (from 60 to 600 C/L/min), which suggests negligible O_2 diffusion limitations to the air cathode. The efficient production of H_2O_2, which oxidizes Fe(II) at nearly 4 orders of magnitude faster than DO,[27, 28] explains why dissolved Fe(II) did not accumulate and GR did not form in the ACAIE system even at the highest CDR of 1200 C/L/min. While no transition from Fe(III) precipitates to GR was observed at in the ACAIE system, some systematic changes in Fe(III) precipitate structure with CDR were detected in the XRD data. At the lowest CDR of 1.5 C/L/min, lepidocrocite was observed in the XRD, but 2LFh became dominant as the CDR increased. This trend in reduced crystallinity can be explained by the decreased efficiency of H_2O_2 production (48 ± 9% of the theoretical value) at CDR of 1.5 C/L/min compared to the high efficiency of H_2O_2 production at CDR> 6 C/L/min. Since <60% of the theoretical H_2O_2 was produced at CDR of 1.5 C/L/min, the half-life of Fe(II) in experiments at low CDR is likely longer than at high CDR. The higher stability of Fe(II) at low CDR is consistent with the well-documented rapid transformation of freshly-formed Fe(III) precipitates to lepidocrocite catalyzed by Fe(II).[52, 53] Another speculative explanation for the difference in the structure of the Fe(III) (oxyhydr)oxides is that long electrolysis times (~6.7 hours) at low CDR

Manuscript accepted on April 20, 2020 for publication in Environmental Science and Technology.
DOI: 10.1021/acs.est.0c00012

of 1.5 C/L/min could allow sufficient time for crystallization of poorly-ordered Fe(III) (oxyhydr)oxides to lepidocrocite by other crystal growth mechanisms (e.g. oriented aggregation or Ostwald ripening).[54]

4.2 Behavior of arsenic in the FeEC and ACAIE systems

In the FeEC experiments, we observed excellent removal of As(III) to below 2 µg/L at the lowest CDR of 1.5 C/L/min (Figure 1A). At this CDR, we also observed the formation of strictly Fe(III)-bearing solids. This effective arsenic removal is explained by complete oxidation of Fe(II) by DO at low rates of Fe(II) addition, which leads to As(III) outcompeting Fe(II) for Fe(IV), resulting in efficient As(III) oxidation and removal.[13, 34, 55] By contrast, as the CDR increased above 6 C/L/min in the FeEC system, we observed nearly 300 µg/L of arsenic, 70 mg/L of Fe and <0.1 mg/L of DO remaining in the solution after electrolysis (Figure 1, Figure S3B). In addition, our structural data revealed the formation of GR. The lower arsenic removal efficiency at high CDR in the FeEC system results from several processes related to the increased Fe(II) addition rate. At high rates of Fe(II) addition, DO is consumed rapidly and leads to the accumulation of aqueous Fe(II), which outcompetes As(III) for reactive Fenton-type oxidants, resulting in inefficient As(III) oxidation. This result is consistent with the As K-edge XANES analysis showing the predominance of sorbed As(III) at CDR >6 C/L/min (Figure 4). In addition, the formation of GR at high CDRs likely decreases arsenic removal efficiency because of its lower

Manuscript accepted on April 20, 2020 for publication in Environmental Science and Technology.
DOI: 10.1021/acs.est.0c00012

specific surface area compared to Fe(III) precipitates and GR could compete with As(III) for the reactive oxidants.[56] Although we still detected inner-sphere As(III) adsorption complexes on GR in the FeEC experiments, our observation that GR did not remove arsenic effectively is consistent with previous work showing Fe(III) precipitates to be more advantageous to arsenic removal.[38]

In contrast to the FeEC system, nearly 100% arsenic removal was observed in ACAIE experiments at all CDRs. For example, aqueous arsenic levels decreased from 1464 μg/L to <4 μg/L, despite the 800-fold shorter treatment time (400 to 0.5 minute electrolysis time for CDR of 1.5 to 1200 C/L/min). In addition, we found no evidence for the accumulation of Fe(II) nor the formation of GR in the ACAIE experiments. The remarkable arsenic removal efficiency of the ACAIE system results can be explained by the rapid kinetics of Fe(II) oxidation by H_2O_2 coupled with higher yields of reactive oxidants. Despite air saturated DO levels observed in the ACAIE system at all dosage rates (Figure S3B), we expect H_2O_2 to outcompete DO to oxidize aqueous Fe(II) ($k_{app\_H2O2} = 10^{4.5}$ $M^{-1}s^{-1}$; $k_{app\_O2} = 10^{0.9}$ $M^{-1}s^{-1}$) because it reacts quicker than DO. We validated this hypothesis with an additional experiment provided in SI (Section S6, Figure S11). The more effective production of reactive oxidants in the ACAIE system is consistent with the As K-edge XANES and EXAFS data, which identified only As(V) bound in the ^{2}C adsorption geometry to Fe(III) precipitate surfaces,

Manuscript accepted on April 20, 2020 for publication in Environmental Science and Technology.
DOI: 10.1021/acs.est.0c00012

regardless of CDR. In addition to efficient oxidation of As(III) to As(V), the lower crystallinity of Fe(III) (oxyhydr)oxides compared to GR formed at high CDR can also benefit arsenic removal because of their high specific surface area.

4.3 Electrolyte composition

Comparing the laboratory experiments, which were conducted primarily in SBGW, with the field experiments performed in real groundwater allows us to examine the influence of groundwater chemistry on arsenic removal in the ACAIE system. For example, previous studies indicate that Ca and Mg aid in the aggregation and flocculation of Fe(III) (oxyhydr)oxides by charge neutralization.[57, 58] Consequently, in the laboratory experiments, high concentrations of Ca and Mg in SBGW likely aided the aggregation of the solids (nominal diameter >0.45μm), resulting in effective particle removal by filtering with measurements of iron and arsenic in the filtered solutions below their respective SMCL and MCL. However, low concentrations of Ca and Mg in Allensworth groundwater prevented the aggregation of Fe(III) (oxyhydr)oxides (nominal size around 0.45 μm), which lead to some of the arsenic-rich Fe(III) (oxyhydr)oxides passing the filters.[59] This was evident by the yellow color of the filtered samples and measurements of arsenic in the filtered solution above the WHO-MCL during electrolysis. However, the addition of alum at the end of electrolysis in the field experiments resulted in the particle flocculation and dissolved

Manuscript accepted on April 20, 2020 for publication in Environmental Science and Technology.
DOI: 10.1021/acs.est.0c00012

iron and arsenic remained far below their respective SMCLs of 0.3 mg/L and 10 µg/L respectively. Dissolved organic carbon in the groundwater could also be responsible for the poor aggregation of Fe(III) (oxyhydr)oxides generated in the field. These results confirm the importance of solution composition (e.g., bivalent cations, dissolved organic carbon) for the removal of particulate iron by filtration. Therefore, an additional coagulation and flocculation step is recommended for particle separation. However, recent studies show that electrocoagulation systems could be coupled with membrane filtration to further decrease treatment times compared to gravitational settling.[60-62]

4.4 Technical and environmental implications

Recent studies show that arsenic levels even below 10 µg/L can cause significant increases in excess cancers, which calls for innovative treatment solutions that can remove arsenic to <1 µg/L.[63] Our results show that ACAIE can achieve arsenic removal <1 µg/L at CDRs of 1.5 and 6 C/L/min. At higher CDRs (and shorter treatment duration) 1 µg/L arsenic can be likely achieved by increasing and optimizing the total charge dose, which is currently under investigation in our laboratory. In addition, ACAIE removes arsenic to <4 µg/L with superior energy efficiency than that of FeEC (Figure S9). The reduction in Electrical Energy per Order for ACAIE, relative to FeEC, ranges from 8% to 76% between CDRs 1.5 to 600 C/L/min (Figure S9). Therefore,

Manuscript accepted on April 20, 2020 for publication in Environmental Science and Technology.
DOI: 10.1021/acs.est.0c00012

target arsenic levels of <1 µg/L can likely be achieved at significantly lower operating costs with ACAIE relative to FeEC. Furthermore, the extremely short treatment duration (i.e. short residence time) implies that ACAIE systems require a much smaller footprint than an equivalent FeEC system. This also could lead to smaller capital cost for the reactor. Based on these benefits, we propose that ACAIE can be a breakthrough technology to decrease arsenic concentrations to less than <1 µg/L both in large-scale water treatment plants in rural communities relying on decentralized treatment.

Importantly, the As K-edge XANES and EXAFS spectra showed that the bonding environment of As(V) did not change with CDR in the ACAIE system, with As(V) forming the ^{2}C adsorption complex with Fe(III) (oxyhydr)oxides in all experiments. Given the wide range of electrolysis times, detection of the same ^{2}C adsorption complex is remarkable. This result is also important since the As and Fe bonding environment in the reaction products of the ACAIE system are nearly identical to arsenic-rich Fe(III) precipitates that have been tested previously for arsenic leachability by the Toxicity Characteristic Leaching Procedure (TCLP)[55, 64] and for long-term disposal by incorporation in concrete.[65, 66] Therefore, the results of previous investigations of the fate of arsenic-rich Fe(III) precipitates during sludge storage and disposal will likely be applicable to the ACAIE

Manuscript accepted on April 20, 2020 for publication in Environmental Science and Technology.
DOI: 10.1021/acs.est.0c00012

treatment residuals, which is useful to inform sludge management strategies.

Low mechanical stability of large size air cathodes could limit the scale-up of ACAIE for single-size very large treatment systems. While mechanical stability can be a concern for single air cathodes of very large size (e.g. larger than a square meter), our field experiments were performed with a modestly large air cathode assembly (air cathode of 400 cm^2) and showed mechanical stability and high efficiency for extended periods. Furthermore, when targeting rural, decentralized communities, small scale ACAIE systems can be implemented with vertically stacked multiple ACAIE reactors, each of moderate scale, without resorting to very large electrodes. However, if eventually larger electrodes are required for much higher capacity ACAIE systems than those in our field tests, screen printing techniques can be explored to fabricate air cathodes with several m^2 surface.

Finally, fouling of the air cathodes can be caused by the precipitation of Ca and Mg carbonates due to local regions of alkaline pH near the cathodes[26] and by the physical accumulation of Fe(III) (oxyhydr)oxides on the cathode surface over months to years of operation. However, we observed no significant change in cathodic H_2O_2 production in waters containing high Ca and Mg concentrations (Figure S10), consistent with previous findings.[26] We note that the impact of fouling by Fe(III) (oxyhydr)oxides on the cathode over long-

Manuscript accepted on April 20, 2020 for publication in Environmental Science and Technology.
DOI: 10.1021/acs.est.0c00012

term continuous operation, which could decrease H_2O_2 production, should be investigated to increase the operational life of the cathodes.

Supporting Information

The supporting information contains: SBGW recipe, air cathode fabrication, Faradaic efficiency of H_2O_2 measurements, energy consumption data, controlled experiments to test the dominant oxidant in ACAIE, X-ray absorption spectroscopy details, long-term performance of the air cathode, in addition to supporting tables and figures referenced in the main manuscript. The supporting information is available free of charge via the internet at http://pubs.acs.org.

Acknowledgements

We acknowledge funding support from Andrew and Virginia Rudd Family Foundation Chair Funds of Prof. Gadgil, CHED funded PCARI project at UC Berkeley, TRDRP project administered by UCOP (Grant no T29IR0649), CERC-WET project supported by the US Department of Energy under award No.DE-IA0000018 at UC Berkeley, Dr. Gadgil's gift funds at LBNL. Synchrotron experiments were performed at SSRL, SLAC National Accelerator Laboratory supported by the U.S. Department of Energy, Office of Science, Basic Energy Sciences, under Contract No. DE-AC02-76SF00515. XRD experiments were performed at Molecular Foundry, LBNL, supported by the Office of Basic Energy

Sciences of the U.S. DOE under Contract No. DE-AC02-05CH11231. We sincerely thank the anonymous reviewers whose comments have improved this manuscript. We are also grateful to James Barazesh, Yanghua Duan, Rachel Scholes and Marc Teixido Planes for valuable discussions and help. Authors are thankful to Jacob Gallego and Jeff Higginbotham from the mechanical engineering student machine shop for their high-quality assistance in the fabrication of ACAIE reactors. SRSB gratefully acknowledges support from CEE Department Block Grant and CEE Nanotechnology Fellowship. SG and DH are grateful for NSF-GRFP Fellowship support.

References

1. Naujokas, M. F.; Anderson, B.; Ahsan, H.; Aposhian, H. V.; Graziano, J. H.; Thompson, C.; Suk, W. A., The Broad Scope of Health Effects from Chronic Arsenic Exposure: Update on a Worldwide Public Health Problem. *Environ Health Persp* **2013,** *121*, (3), 295-302.
2. Murcott, S., *Arsenic contamination in the world*. IWA publishing: 2012.
3. Steinmaus, C. M.; Ferreccio, C.; Romo, J. A.; Yuan, Y.; Cortes, S.; Marshall, G.; Moore, L. E.; Balmes, J. R.; Liaw, J.; Golden, T.; Smith, A. H., Drinking water arsenic in northern chile: high cancer risks 40 years after exposure cessation. *Cancer Epidemiol Biomarkers Prev* **2013,** *22*, (4), 623-30.
4. Smith, A. H.; Lopipero, P. A.; Bates, M. N.; Steinmaus, C. M., Public health - Arsenic epidemiology and drinking water standards. *Science* **2002,** *296*, (5576), 2145-2146.
5. Smith, A. H.; Hopenhayn-Rich, C.; Bates, M. N.; Goeden, H. M.; Hertz-Picciotto, I.; Duggan, H. M.; Wood, R.; Kosnett, M. J.; Smith, M. T., Cancer risks from arsenic in drinking water. *Environ Health Perspect* **1992,** *97*, 259-67.
6. Chakraborti, D.; Rahman, M. M.; Chatterjee, A.; Das, D.; Das, B.; Nayak, B.; Pal, A.; Chowdhury, U. K.; Ahmed, S.; Biswas, B. K.; Sengupta, M. K.; Lodh, D.; Samanta, G.; Chakraborty, S.; Roy, M. M.; Dutta, R. N.; Saha, K. C.; Mukherjee, S. C.; Pati, S.; Kar, P. B., Fate of over 480 million inhabitants living in arsenic and fluoride endemic

Manuscript accepted on April 20, 2020 for publication in Environmental Science and Technology.
DOI: 10.1021/acs.est.0c00012

761 Indian districts: Magnitude, health, socio-economic effects and
762 mitigation approaches. *J Trace Elem Med Bio* **2016,** *38*, 33-45.
763 7. Johnston, R. B.; Hanchett, S.; Khan, M. H., The socio-economics of
764 arsenic removal. *Nat Geosci* **2010,** *3*, (1), 2-3.
765 8. Amrose, S.; Burt, Z.; Ray, I., Safe Drinking Water for Low-Income
766 Regions. *Annu Rev Env Resour* **2015,** *40*, 203-231.
767 9. Kumar, P. R.; Chaudhari, S.; Khilar, K. C.; Mahajan, S. P., Removal
768 of arsenic from water by electrocoagulation. *Chemosphere* **2004,** *55*,
769 (9), 1245-1252.
770 10. Hernandez, D.; Boden, K.; Paul, P.; Bandaru, S.; Mypati, S.; Roy,
771 A.; Amrose, S.; Roy, J.; Gadgil, A., Strategies for successful field
772 deployment in a resource-poor region: Arsenic remediation technology
773 for drinking water. *Development Engineering* **2019,** *4*, 100045.
774 11. Amrose, S. E.; Bandaru, S. R. S.; Delaire, C.; van Genuchten, C.
775 M.; Dutta, A.; DebSarkar, A.; Orr, C.; Roy, J.; Das, A.; Gadgil, A. J.,
776 Electro-chemical arsenic remediation: Field trials in West Bengal. *Sci*
777 *Total Environ* **2014,** *488*, 543-550.
778 12. Lakshmanan, D.; Clifford, D. A.; Samanta, G., Ferrous and Ferric
779 Ion Generation During Iron Electrocoagulation. *Environ Sci Technol*
780 **2009,** *43*, (10), 3853-3859.
781 13. Hug, S. J.; Leupin, O., Iron-catalyzed oxidation of arsenic(III) by
782 oxygen and by hydrogen peroxide: pH-dependent formation of
783 oxidants in the Fenton reaction. *Environ Sci Technol* **2003,** *37*, (12),
784 2734-2742.
785 14. Roberts, L. C.; Hug, S. J.; Ruettimann, T.; Billah, M.; Khan, A. W.;
786 Rahman, M. T., Arsenic removal with iron(II) and iron(III) in waters with
787 high silicate and phosphate concentrations. *Environ Sci Technol* **2004,**
788 *38*, (1), 307-15.
789 15. Lu, H. F.; Chen, H. F.; Kao, C. L.; Chao, I.; Chen, H. Y., A
790 computational study of the Fenton reaction in different pH ranges.
791 *Phys Chem Chem Phys* **2018,** *20*, (35), 22890-22901.
792 16. Wiegand, H. L.; Orths, C. T.; Kerpen, K.; Lutze, H. V.; Schmidt, T.
793 C., Investigation of the Iron-Peroxo Complex in the Fenton Reaction:
794 Kinetic Indication, Decay Kinetics, and Hydroxyl Radical Yields. *Environ*
795 *Sci Technol* **2017,** *51*, (24), 14321-14329.
796 17. Bataineh, H.; Pestovsky, O.; Bakac, A., pH-induced mechanistic
797 changeover from hydroxyl radicals to iron(IV) in the Fenton reaction.
798 *Chem Sci* **2012,** *3*, (5), 1594-1599.
799 18. Delaire, C.; Amrose, S.; Zhang, M. H.; Hake, J.; Gadgil, A., How do
800 operating conditions affect As(III) removal by iron electrocoagulation?
801 *Water Res* **2017,** *112*, 185-194.
802 19. van Genuchten, C. M.; Behrends, T.; Stipp, S. L. S.; Dideriksen, K.,
803 Achieving arsenic concentrations of <1mug/L by Fe(0) electrolysis: The
804 exceptional performance of magnetite. *Water Res* **2020,** *168*, 115170.

20. Dubrawski, K. L.; van Genuchten, C. M.; Delaire, C.; Amrose, S. E.; Gadgil, A. J.; Mohseni, M., Production and Transformation of Mixed-Valent Nanoparticles Generated by Fe(0) Electrocoagulation. *Environ Sci Technol* **2015,** *49*, (4), 2171-2179.
21. van Genuchten, C. M.; Behrends, T.; Kraal, P.; Stipp, S. L. S.; Dideriksen, K., Controls on the formation of Fe(II,III) (hydr)oxides by Fe(0) electrolysis. *Electrochim Acta* **2018,** *286*, 324-338.
22. Jiang, Y. Y.; Ni, P. J.; Chen, C. X.; Lu, Y. Z.; Yang, P.; Kong, B.; Fisher, A.; Wang, X., Selective Electrochemical H2O2 Production through Two-Electron Oxygen Electrochemistry. *Adv Energy Mater* **2018,** *8*, (31), 1801909.
23. Rozendal, R. A.; Leone, E.; Keller, J.; Rabaey, K., Efficient hydrogen peroxide generation from organic matter in a bioelectrochemical system. *Electrochem Commun* **2009,** *11*, (9), 1752-1755.
24. Xia, C.; Xia, Y.; Zhu, P.; Fan, L.; Wang, H., Direct electrosynthesis of pure aqueous H2O2 solutions up to 20% by weight using a solid electrolyte. *Science* **2019,** *366*, (6462), 226-231.
25. Cheng, S.; Liu, H.; Logan, B. E., Increased performance of single-chamber microbial fuel cells using an improved cathode structure. *Electrochem Commun* **2006,** *8*, (3), 489-494.
26. Barazesh, J. M.; Hennebel, T.; Jasper, J. T.; Sedlak, D. L., Modular Advanced Oxidation Process Enabled by Cathodic Hydrogen Peroxide Production. *Environ Sci Technol* **2015,** *49*, (12), 7391-7399.
27. King, D. W.; Farlow, R., Role of carbonate speciation on the oxidation of Fe(II) by H2O2. *Mar Chem* **2000,** *70*, (1-3), 201-209.
28. King, D. W., Role of carbonate speciation on the oxidation rate of Fe(II) in aquatic systems. *Environ Sci Technol* **1998,** *32*, (19), 2997-3003.
29. Si, Y. X.; Li, G. H.; Zhang, F., Energy-Efficient Oxidation and Removal of Arsenite from Groundwater Using Air-Cathode Iron Electrocoagulation. *Environ Sci Tech Let* **2017,** *4*, (2), 71-75.
30. Hering, J. G.; Katsoyiannis, I. A.; Theoduloz, G. A.; Berg, M.; Hug, S. J., Arsenic Removal from Drinking Water: Experiences with Technologies and Constraints in Practice. *J Environ Eng* **2017,** *143*, (5), 03117002.
31. Dixit, S.; Hering, J. G., Comparison of arsenic(V) and arsenic(III) sorption onto iron oxide minerals: Implications for arsenic mobility. *Environ Sci Technol* **2003,** *37*, (18), 4182-4189.
32. Huhmann, B. L.; Neumann, A.; Boyanov, M. I.; Kemner, K. M.; Scherer, M. M., Emerging investigator series: As(v) in magnetite: incorporation and redistribution. *Environ Sci-Proc Imp* **2017,** *19*, (10), 1208-1219.
33. Delaire, C.; van Genuchten, C. M.; Nelson, K. L.; Amrose, S. E.; Gadgil, A. J., Escherichia coli Attenuation by Fe Electrocoagulation in

Synthetic Bengal Groundwater: Effect of pH and Natural Organic Matter. *Environ Sci Technol* **2015,** *49*, (16), 9945-9953.
34. Li, L.; van Genuchten, C. M.; Addy, S. E. A.; Yao, J. J.; Gao, N. Y.; Gadgil, A. J., Modeling As(III) Oxidation and Removal with Iron Electrocoagulation in Groundwater. *Environ Sci Technol* **2012,** *46*, (21), 12038-12045.
35. Hansen, H. C. B., Composition, Stabilization, and Light-Absorption of Fe(Ii)Fe(Iii) Hydroxy-Carbonate (Green Rust). *Clay Miner* **1989,** *24*, (4), 663-669.
36. Webb, S., SIXPACK: a graphical user interface for XAS analysis using IFEFFIT. *Physica Scripta* **2005,** *T115*, 1011-1014.
37. van Genuchten, C.; Addy, S.; Pena, J.; Gadgil, A., Removing arsenic from synthetic groundwater with iron electrocoagulation: An Fe and As K-edge EXAFS study. *Environmental Science & Technology* **2012,** *46*, (2), 986-994.
38. van Genuchten, C. M.; Behrends, T.; Dideriksen, K., Emerging investigator series: interdependency of green rust transformation and the partitioning and binding mode of arsenic. *Environ Sci Process Impacts* **2019,** *21*, (9), 1459-1476.
39. Newville, M., IFEFFIT: interactive XAFS analysis and FEFF fitting. *J Synchrotron Radiat* **2001,** *8*, (Pt 2), 322-4.
40. Jonsson, J.; Sherman, D. M., Sorption of As(III) and As(V) to siderite, green rust (fougerite) and magnetite: Implications for arsenic release in anoxic groundwaters. *Chem Geol* **2008,** *255*, (1-2), 173-181.
41. Rehr, J. J.; Albers, R. C.; Zabinsky, S. I., High-order multiple-scattering calculations of x-ray-absorption fine structure. *Phys Rev Lett* **1992,** *69*, (23), 3397-3400.
42. Kitahama, K.; Kiriyama, R.; Baba, Y., Refinement of Crystal-Structure of Scorodite. *Acta Crystallogr B* **1975,** *31*, (Jan15), 322-324.
43. Downs, R. T.; Hall-Wallace, M., The American Mineralogist crystal structure database. *American Mineralogist* **2003,** *88*, (1), 247-250.
44. Ruby, C.; Usman, M.; Naille, S.; Hanna, K.; Carteret, C.; Mullet, M.; Francois, M.; Abdelmoula, M., Synthesis and transformation of iron-based layered double hydroxides. *Appl Clay Sci* **2010,** *48*, (1-2), 195-202.
45. Liu, A. R.; Liu, J.; Pan, B. C.; Zhang, W. X., Formation of lepidocrocite (gamma-FeOOH) from oxidation of nanoscale zero-valent iron (nZVI) in oxygenated water. *Rsc Adv* **2014,** *4*, (101), 57377-57382.
46. Su, C. M.; Wilkin, R. T., Arsenate and arsenite sorption on and arsenite oxidation by iron(II, III) hydroxycarbonate green rust. *Acs Sym Ser* **2005,** *915*, 25-40.
47. Voegelin, A.; Kaegi, R.; Frommer, J.; Vantelon, D.; Hug, S. J., Effect of phosphate, silicate, and Ca on Fe(III)-precipitates formed in

aerated Fe(II)- and As(III)-containing water studied by X-ray absorption spectroscopy. *Geochim Cosmochim Ac* **2010,** *74*, (1), 164-186.
48. Ona-Nguema, G.; Morin, G.; Juillot, F.; Calas, G.; Brown, G. E., EXAFS analysis of arsenite adsorption onto two-line ferrihydrite, hematite, goethite, and lepidocrocite. *Environ Sci Technol* **2005,** *39*, (23), 9147-9155.
49. Waychunas, G. A.; Rea, B. A.; Fuller, C. C.; Davis, J. A., Surface-chemistry of ferrihydrite .1. Exafs studies of the geometry of coprecipitated and adsorbed arsenate. *Geochim Cosmochim Ac* **1993,** *57*, (10), 2251-2269.
50. Michel, F. M.; Ehm, L.; Antao, S. M.; Lee, P. L.; Chupas, P. J.; Liu, G.; Strongin, D. R.; Schoonen, M. A. A.; Phillips, B. L.; Parise, J. B., The structure of ferrihydrite, a nanocrystalline material. *Science* **2007,** *316*, (5832), 1726-1729.
51. Trolard, F.; Bourrie, G.; Abdelmoula, M.; Refait, P.; Feder, F., Fougerite, a new mineral of the pyroaurite-iowaite group: Description and crystal structure. *Clay Clay Miner* **2007,** *55*, (3), 323-334.
52. Pedersen, H.; Postma, D.; Jakobsen, R.; Larsen, O., Fast transformation of iron oxyhydroxides by the catalytic action of aqueous Fe(II). *Geochim Cosmochim Ac* **2005,** *69*, (16), 3967-3977.
53. Liu, H.; Li, P.; Zhu, M.; Wei, Y.; Sun, Y., Fe(II)-induced transformation from ferrihydrite to lepidocrocite and goethite. *Journal of Solid State Chemistry* **2007,** *180*, (7), 2121-2128.
54. Cornell, R. M.; Schwertmann, U., *The iron oxides: structure, properties, reactions, occurrences and uses*. John Wiley & Sons: 2003.
55. Amrose, S.; Gadgil, A.; Srinivasan, V.; Kowolik, K.; Muller, M.; Huang, J.; Kostecki, R., Arsenic removal from groundwater using iron electrocoagulation: Effect of charge dosage rate. *J Environ Sci Heal A* **2013,** *48*, (9), 1019-1030.
56. Usman, M.; Abdelmoula, M.; Hanna, K.; Gregoire, B.; Faure, P.; Ruby, C., Fe-II induced mineralogical transformations of ferric oxyhydroxides into magnetite of variable stoichiometry and morphology. *Journal of Solid State Chemistry* **2012,** *194*, 328-335.
57. Zhang, Y. Y.; She, X. W.; Gao, X.; Shan, C.; Pan, B. C., Unexpected Favorable Role of Ca2+ in Phosphate Removal by Using Nanosized Ferric Oxides Confined in Porous Polystyrene Beads. *Environ Sci Technol* **2019,** *53*, (1), 365-372.
58. van Genuchten, C. M.; Pena, J.; Amrose, S. E.; Gadgil, A. J., Structure of Fe(III) precipitates generated by the electrolytic dissolution of Fe(0) in the presence of groundwater ions. *Geochim Cosmochim Ac* **2014,** *127*, 285-304.
59. van Genuchten, C. M.; Gadgil, A. J.; Pena, J., Fe(III) Nucleation in the Presence of Bivalent Cations and Oxyanions Leads to Subnanoscale 7 angstrom Polymers. *Environ Sci Technol* **2014,** *48*, (20), 11828-11836.

Manuscript accepted on April 20, 2020 for publication in Environmental Science and Technology.
DOI: 10.1021/acs.est.0c00012

939 60. Ghurye, G.; Clifford, D.; Tripp, A., Iron coagulation and direct
940 microfiltration to remove arsenic from groundwater. *J Am Water Works*
941 *Ass* **2004,** *96*, (4), 143-152.
942 61. Zouboulis, A.; Katsoyiannis, I., Removal of arsenates from
943 contaminated water by coagulation-direct filtration. *Separ Sci Technol*
944 **2002,** *37*, (12), 2859-2873.
945 62. Ahmad, A.; Rutten, S.; de Waal, L.; Vollaard, P.; van Genuchten,
946 C.; Bruning, H.; Cornelissen, E.; van der Wal, A., Mechanisms of
947 arsenate removal and membrane fouling in ferric based
948 coprecipitation–low pressure membrane filtration systems. *Sep Purif*
949 *Technol* **2020,** *241*, 116644.
950 63. Ahmad, A.; van der Wens, P.; Baken, K.; de Waal, L.;
951 Bhattacharya, P.; Stuyfzand, P., Arsenic reduction to< 1 µg/L in Dutch
952 drinking water. *Environment International* **2020,** *134*, 105253.
953 64. Xie, S. W.; Yuan, S. H.; Liao, P.; Tong, M.; Gan, Y. Q.; Wang, Y. X.,
954 Iron-Anode Enhanced Sand Filter for Arsenic Removal from Tube Well
955 Water. *Environ Sci Technol* **2017,** *51*, (2), 889-896.
956 65. Roy, A.; van Genuchten, C. M.; Mookherje, I.; Debsarkar, A.;
957 Dutta, A., Concrete stabilization of arsenic-bearing iron sludge
958 generated from an electrochemical arsenic remediation plant. *J Environ*
959 *Manage* **2019,** *233*, 141-150.
960 66. Clancy, T. M.; Snyder, K. V.; Reddy, R.; Lanzirotti, A.; Amrose, S.
961 E.; Raskin, L.; Hayes, K. F., Evaluating the cement stabilization of
962 arsenic-bearing iron wastes from drinking water treatment. *J Hazard*
963 *Mater* **2015,** *300*, 522-529.
964

965

966 **Figure FOR TABLE OF CONTENTS ONLY**

967

Manuscript accepted on April 20, 2020 for publication in Environmental Science and Technology.
DOI: 10.1021/acs.est.0c00012

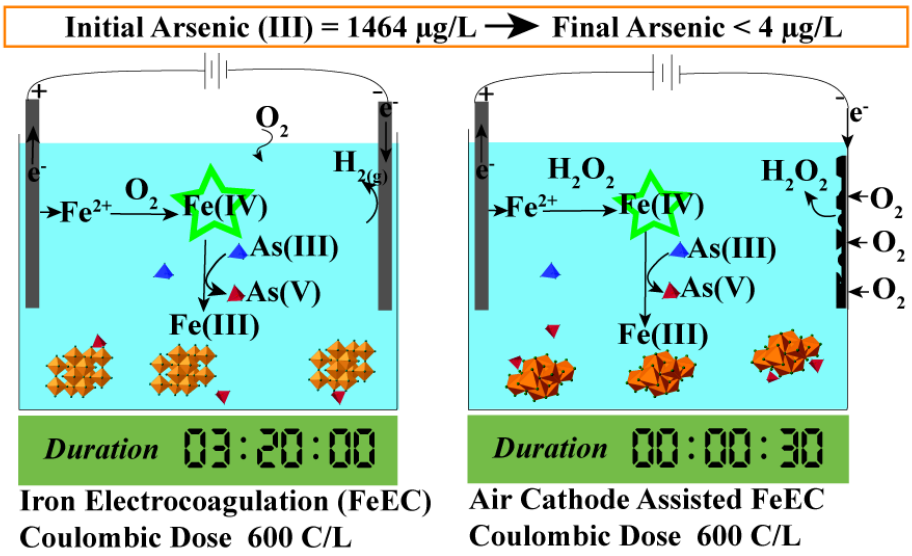

968